ACS APPLIED MATERIALS & INTERFACES

LETTER

www.acsami.org

Hole Transparent and Hole Blocking Transport in Single-Crystal-Like Organic Heterojunction: When Rods Hold up Disks

Feng Zhu,[†] Mandy Grobosch,[†] Uwe Treske,[†] Lizhen Huang,[‡] Weichao Chen,[‡] Jianbing Yang,[‡] Donghang Yan,[‡] and Martin Knupfer*[,†]

[†]Leibniz Institute of Solid State and Materials Research Dresden, D-01069 Dresden, Germany

[‡]Changchun Institute of Applied Chemistry, Chinese Academy of Sciences, 130022 Changchun, China

ABSTRACT: Single-crystal-like organic heterojuntions are fabricated with disk-like molecules and different rodlike molecules. Hole transparent and blocking transport are demonstrated with photoemission spectroscopy and field-effect transistors. These results demonstrate a route to utilize adjustable interfacial electronic structure and control transport behavior in developing functional organic crystalline devices and crystalline nanocircuits.

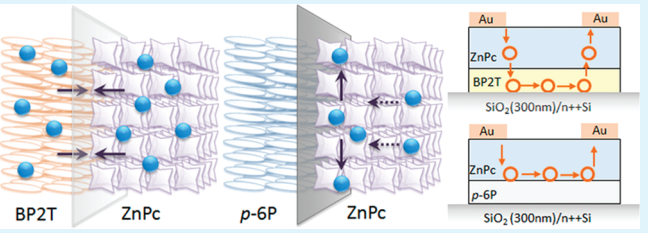

KEYWORDS: photoemission spectroscopy, organic semiconductors, epitaxy growth, organic heterojunction interface, organic field-effect transistors

INTRODUCTION

Semiconductor heterojunctions are of great importance in modern electronics industry as they are part of almost every device. Molecular heterostructures recently have attracted a lot of attention because of their promising potential application in developing large-area functional devices and nanolevel devices, such as transistors, molecular chips and nanocircuits. Within the rapid progress in the fields of nanoelectronics and molecular electronics, the heteroepitaxial growth of molecular films, highly ordered nanostructures, crystalline organic superlattices and heteronanoribbons have been demonstrated and prove the feasibility of tailoring organic heterostructures.[1−5] However, the realization of adjustable interfacial electronic structures in crystalline organic heterostructures has become an emergent task, due to the variety of potential devices and functionalities. In particular, one aim is to be able to tune the charge carrier transport behavior via the properties of crystalline heterostructures and develop new type of functional solid-state devices, for instance, organic laser devices. Compared to the efforts taken on amorphous or low-quality-film organic/metal and organic/organic interfaces in past decades;[6−15] however, only a few reports have addressed the intrinsic interfacial electronic properties of single-crystal-like molecular heterostructures. One reason is that there is still no widely recognized method of fabricating organic heterostructure crystals. Furthermore, recent reports indicate that crystalline molecular films and oriented molecule assemblies demonstrate an orientation dependence of their electronic structure or even features of energy band dispersion, which is clearly distinguished from the unique energy levels of the individual molecule and also make the electronic properties of the heterostructure more complicated.[16−21] In this contribution, we focus on the investigation of the interfacial electronic structure of single-crystal-like organic heterojunctions and demonstrate crystalline heterojunction systems, which either are transparent for holes or efficiently block hole transport across the interface.

P-type organic semiconductors 2,5-bis(4-biphenylyl) bithiophene (BP2T), *p*-sexiphenyl (*p*-6P), and zinc phthalocyanine (ZnPc) are selected, as they are archetype representatives of rod-like and disk-like hole-transport materials with excellent (opto)electronic properties (see Figure 1).[22−25] The "Weak epitaxy growth" (WEG) method was employed to fabricate crystalline heterojunction films of ZnPc/BP2T and ZnPc/*p*-6P composition.[26,27] Using this method, the epitaxial growth of the disk-like molecules, ZnPc, can be achieved on the well ordered layers of the rod-like molecules BP2T and *p*-6P. To obtain a complete picture of the electronic structure of these representative crystalline organic heterostructures, photoemission spectroscopy (PES) measurements were carried out during fabrication of the two crystalline heterojunctions, and charge transport studies have been performed using organic thin film transistors (OTFT).

EXPERIMENTAL SECTION

Materials and Film Growth. The commercial material ZnPc was purchased from Aldrich Co. BP2T and *p*-6P were synthesized according to refs 28 and 29, respectively. The weak epitaxy growth (WEG) method was used to fabricate high-crystalline heterojunction films, and the details were described in refs 26 and ref 27.

Photoemission Spectroscopy Measurements. The photoemission spectroscopy experiments were carried out using a commercial PHOIBOS-150 (SPECS) ultrahigh vacuum (UHV)

Received: April 26, 2011
Accepted: June 14, 2011
Published: June 14, 2011

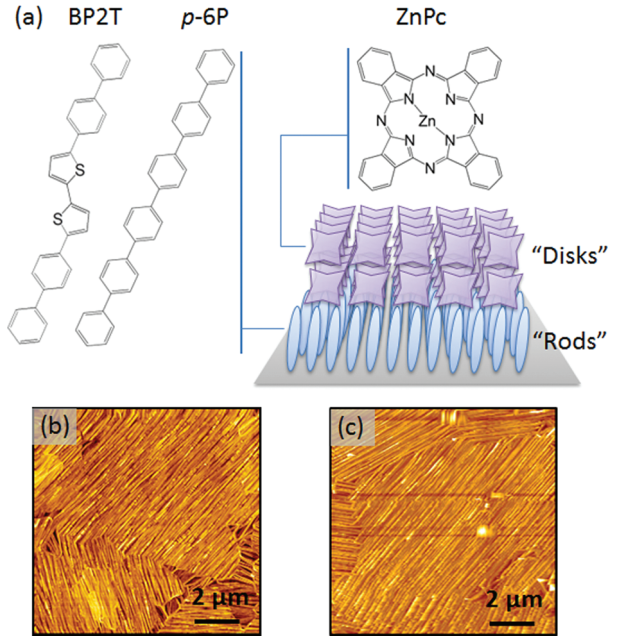

Figure 1. (a) Molecular structure of ZnPc, BP2T, and *p*-6P. Schematic diagram of weak epitaxy growth of disklike molecules on rodlike molecules. (b, c) AFM image of ZnPc/BP2T and ZnPc/p-6P, respectively.

surface analysis system with a sample preparation and an measuring chamber, each with a base pressure of $\sim 2 \times 10^{-10}$ mbar. A cleaned n-type Si wafer with a native oxide layer on top was used as substrate. The Si wafer was heated in the preparation chamber for 30 min at 300 °C to remove surface contaminations before depositing the molecules. At a substrate temperature of 100 °C, the organic materials were deposited successively. The film thickness was monitored with a quartz crystal oscillator. After each deposition step, the samples were transferred into the measurement chamber without breaking the vacuum. The PHOIBOS-150 (SPECS) spectrometer is equipped with a He-discharge lamp and a monochromatic Al Kα source provide photons with 21.22 eV for UPS (ultraviolet photoemission spectroscopy) and 1486.6 eV for XPS (X-ray photoemission spectroscopy), respectively. The total energy resolution of the spectrometer is about 0.1 eV (UPS) and 0.35 eV (XPS). For UPS the samples were measured under a bias of 7 V. For XPS the energy scale was calibrated to reproduce the binding energy of Au4f$_{7/2}$ (84.0 eV). The attenuation of the intensity of the Si2p peak was used to check the thickness of the BP2T (*p*-6P) layer and ZnPc layers, respectively.[30,31] After the PES measurements, the samples were transferred out of the chamber. Immediately, the morphology of the films was imaged with a SPI3800N atomic force microscope (Seiko Instruments Inc.) using the tapping mode.

Fabrication and Characterization of OTFTs. OTFTs of ZnPc(20 nm)/BP2T(6 nm) and ZnPc(20 nm)/*p*-6P(6 nm) were fabricated using the WEG method on an n-type silicon wafer with a 300 nm thermal oxidation SiO_2 layer as gate insulator. After the growth of WEG films, source/drain Au electrodes were fabricated. The length and width of the transistor channel was 0.2 mm and 6.0 mm, respectively. The current−voltage characterisitics of the transistors were measured with two Keithley 236 source measurement units under ambient conditions at room temperature. The field-effect mobilities were obtained using the transfer curves under the bias of $V_{DS} = -50$ V through the equation $ID = (\mu C_i W)/(2L)(V_{GS} - V_{th})^2$.

RESULTS AND DISCUSSION

We take the ZnPc/BP2T system to introduce the procedure of our experiments and the analysis of the photoemission spectra. First, BP2T molecules were deposited on a cleaned Si-wafer with a native oxide layer step by step taking advantage of the weak epitaxy growth condition, the coverage increases from less than a monolayer (2.0 nm) to more than 2 monolayers (6.8 nm). Subsequently, 7.4 nm ZnPc were deposited on the BP2T layer again in various steps. After each deposition, the samples were transferred to the measuring chamber and characterized by ultraviolet photoemission (UPS) and X-ray photoemission (XPS) measurements without breaking the vacuum.

During the deposition of BP2T molecules on the substrate, the BP2T molecules grow in a standing-up mode and form smooth layer-by-layer thin films. The large-area BP2T molecular domains aggregate to form continuous uniform films and the (002) planes maintain parallel to the substrate.[27] The thickness of the BP2T layer indicates that besides two complete layers of BP2T, a third layer is also present at some locations of the sample. Induced by the BP2T layers, the subsequently deposited ZnPc molecules demonstrate weak epitaxy growth behavior, and the ZnPc molecules arrange along the [110] and [$\bar{1}$10] geometry channel of the BP2T surface, which corresponds to the incommensurate epitaxial mode,[27] whereas on the surface of three monolayers of BP2T, the ZnPc molecules demonstrate the commensurate epitaxial mode. The details of this molecular growth mechanism are described in refs 26 and 27. Finally, with increasing thickness of ZnPc, the continuous single-crystal-like heterostructure ZnPc/BP2T is formed. Similarly, we can obtain crystalline ZnPc/*p*-6P systems. The morphology of ZnPc/BP2T and ZnPc/*p*-6P were imaged with atomic force microscopy (AFM) after the PES measurements. As shown in panels b and c in Figure 1, induced by BP2T and *p*-6P molecules, the growth of ZnPc molecules exhibit WEG behavior. Large-area crystalline domains aggregated smoothly to form a highly ordered layer,

During the formation of single-crystal-like hole-transport junctions, the detailed interfacial electronic structure can be obtained with photoemission spectroscopy measurements. The molecular orbital alignment, the work function Φ, the interface dipole Δ, the ionization potential (IP) and the hole injection barriers (HIB) are extracted from the spectra. The details of the analysis of these parameters have been thoroughly described in several reviews.[8,10,32] Figure 2 illustrates the valence-band PES results taken for the ZnPc/BP2T and ZnPc/*p*-6P systems. For comparison, the intensity was normalized to the height of the most intense spectral feature. The bottom spectrum in each panel is representative of the cleaned n-Si wafer with a native oxide layer, the Fermi level of which is pinned to the work function of the substrate. When the monolayer of BP2T is formed, the highest occupied molecular orbital (HOMO) peak can be clearly observed. Meanwhile, there is a shift of the secondary-electron cutoff and thereafter no obvious binding energy change with increasing BP2T layer thickness is observed. When the ZnPc layer was deposited step-by-step, as shown in right panel of Figure 2a, the HOMO-1 peak of BP2T becomes weak and disappears after 2.4 nm of ZnPc, which indicates the effective coverage by a ZnPc layer. At the same time, the

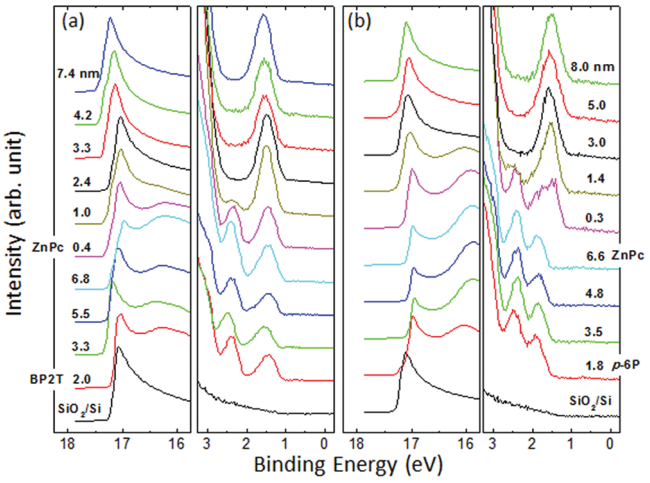

Figure 2. Evolution of the secondary electron cutoff and the HOMO region of the valence band PES spectra of (a) ZnPc/BP2T and (b) ZnPc/*p*-6P.

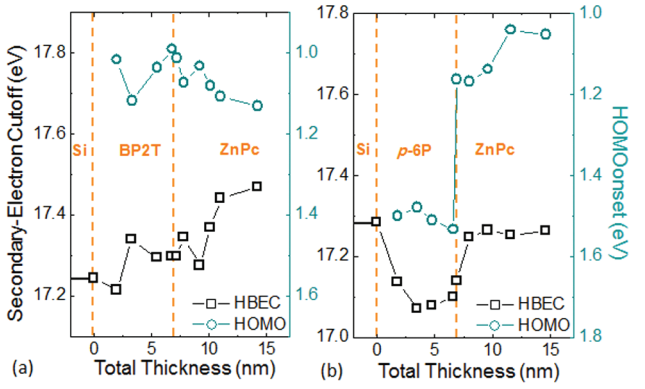

Figure 3. Plot of the secondary-electron cutoff (high binding energy cutoff (HBEC)) and HOMO onset position in the PES spectra of (a) ZnPc/BP2T and (b) ZnPc/*p*-6P.

component of the ZnPc HOMO is strengthened. Therefore, the onset of the HOMO only represents ZnPc, which shifts about 0.1 eV to the high binding energy direction until 7.4 nm (Figure 3a). The X-ray photoemission spectra were also carried out to investigate the evolution of core levels in the hetero-structures. The spectral features of N1s, Zn2$p_{3/2}$, and S2p core levels do not show obvious changes and only vary in the range of the experimental error. Furthermore, there is no new peak appearing during the growth process. This clearly indicates that the interaction between BP2T and ZnPc is of physisorption character. The results from the photoemission measurements are summarized in Figure 3, and they allow to derive the interfacial electronic structure of ZnPc/BP2T, which is shown in Figure 4a in a schematic energy level diagram. An equivalent experiment and data analysis have been carried out for the ZnPc/*p*-6P system (Figure 4b). It is worth to note that although the energy shift of 0.1 eV of the HOMO onset of ZnPc is comparable to the resolution of UPS, herein we temporarily suggest this shift indicates a weak energy level bending instead of a complete interfacial dipole, because both the secondary-electron cutoff and the HOMO onset position shift gradually in a range of more than 5 nm. The IP of BP2T and ZnPc obtained in this experiment is 5.0 and 4.9 eV, respectively. From previously reported PES data

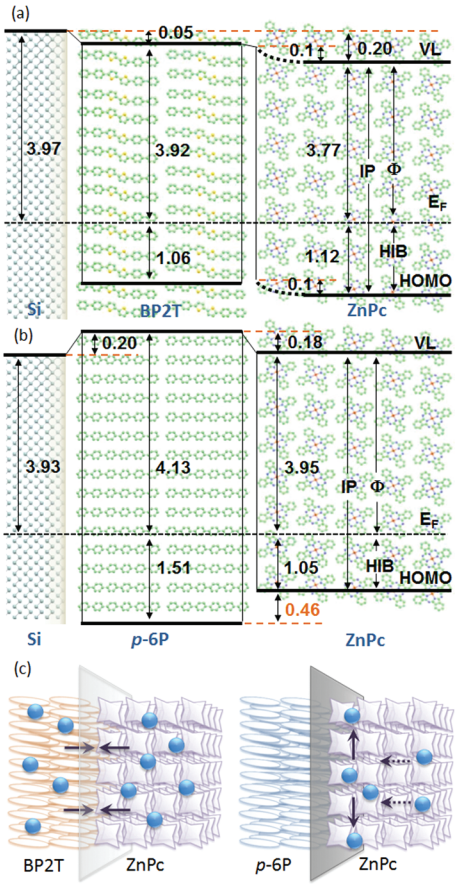

Figure 4. Schematic energy level diagrams of the single-crystal-like heterostructure of (a) ZnPc/BP2T and (b) ZnPc/*p*-6P. Energy values are in unit of electronvolt (eV). (c) Schematic diagram of hole transparent transport through the ZnPc/BP2T interface and hole blocking at the ZnPc/*p*-6P interface.

of BP2T and ZnPc,[33,34] we know that before the materials are brought into contact, the Fermi energy of the n-doped Si wafer is in the energy gap of each material. Under this condition, according to various models[11,13,35,36] that have been proposed for the description of organic interfacial electronic properties, the vacuum level of ZnPc and BP2T should be aligned very close to that of the substrate, and the HOMO of BP2T should be lower than that of ZnPc. This prediction obviously conflicts with the PES results of our single-crystal-like heterojunctions. Generally, it is assumed that the final alignment of energy levels in O/O interfaces is determined by the equilibrium of electrons in certain energy levels at either side of the interface. Therefore, the energy level alignment of crystalline ZnPc/BP2T can in principle be interpreted as the result of charge equilibrium between substrate and heterostructure interfaces, although the exact mechanisms for high-crystalline organic heterostructures are not clear yet.

It is very important to realize that due to the continuity and compactness of the single-crystal-like films, deep traps and other energy levels resulting from imperfect films do not play a dominant role,[37] so that holes will be mainly transported in the valence bands of the crystals. Although the IP of crystalline ZnPc is smaller than that of the crystalline BP2T layer, when the heterostructure is formed, the HOMO of ZnPc is almost perfectly aligned to that of BP2T. As shown in Figure 4a, the HIB between BP2T and ZnPc is within 0.1 eV. Consequently,

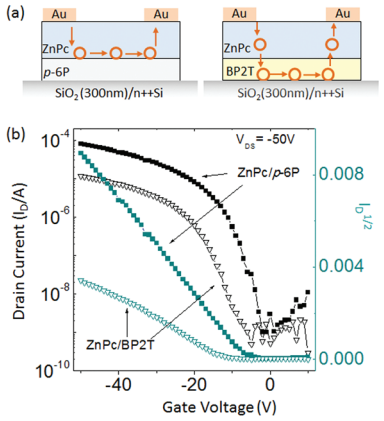

Figure 5. (a) Thin-film transistors of ZnPc/*p*-6P (left panel) and ZnPc/BP2T (right panel). (b) Transfer characteristic curves under $V_{DS} = -50$ V. The corresponding curves of the square root of the drain current are used to extract the field-effect mobility.

holes can easily flow in two directions, either from BP2T to ZnPc or vice versa, which can be described in terms of a transparent interface for holes (see left panel of Figure 4c). In contrast, in the ZnPc/*p*-6P system (Figure 4b), the HIB between *p*-6P and ZnPc is substantially larger (about 0.46 eV). In this case, we expect this energy barrier to effectively block the holes when flowing from ZnPc to *p*-6P (right panel of Figure 4c).

The interfacial electronic structures obtained above indicate that organic heterojunctions can be easily tuned to adjust the hole transport in crystalline heterojunctions devices and nanocircuits by choosing the organic substituents without losing the high crystallinity. Generally speaking, to measure the current–voltage characteristics of a diode device is the most effetive demonstration of charge transport behavior.[38] However, the electronic properties of two organic/electrode interfaces will make the transport process in heterojunction diodes more complex, which depresses the effect of heterojunction intefaces. Here, we demonstrate the different functionalities of single-crystal-like ZnPc/BP2T and ZnPc/*p*-6P junctions using OTFTs, which were fabricated on an n-doped Si wafer with a 300 nm SiO_2 layer on top and tested under ambient condition (Figure 5a). The two transistors both are characterized by hole transport behavior, and the field-effect mobilities were extracted from the transfer characteristic curves at saturation region (Figure 5b). For the ZnPc/*p*-6P transistors, the mobility reaches values as high as 0.30 $cm^2\ V^{-1}\ s^{-1}$, in accordance with previous reports.[26] Contrary, for the ZnPc/BP2T transistors, the field-effect mobility only is 0.07 $cm^2\ V^{-1}\ s^{-1}$. The reason of this large difference can now be rationalized using the energy level diagram of the two systems as derived with our photoemission studies. As described above, the HIB between ZnPc and *p*-6P is about 0.46 eV, which is significantly larger than that of ZnPc/BP2T. Then, in the transistor based upon the ZnPc/*p*-6P system holes injected from the source electrode under a negative bias are blocked by this barrier. Thus, the induced holes flow in the ZnPc layer right at ZnPc/*p*-6P interface. Therefore, the field-effect mobility of 0.3 $cm^2\ V^{-1}\ s^{-1}$ reflects the properties of single-crystal-like ZnPc layer.

In contrast, for the ZnPc/BP2T system, the injected holes easily cross the organic heterointerface and the BP2T layer is the working channel of the corresponding OTFT, i.e., the induced holes move in a range of 2 nm from the BP2T/SiO_2 interface.[39] Consequently, the field-effect mobility of 0.07 $cm^2\ V^{-1}\ s^{-1}$ reflects the charge transport behavior in the BP2T layer. This is schematically summarized in Figure 5a. We infer that the ZnPc/BP2T system is very well suited to be used in devices utilizing charge transport in the direction perpendicular to the interface. Indeed, as reported previously,[40] in C_{60}/ZnPc/BP2T solar cells, the donor part ZnPc/BP2T exhibits very favorable hole transport behavior.

CONCLUSION

The combined results from PES and OTFTs above strongly indicate that although crystalline ZnPc molecular layers growing on BP2T and *p*-6P layer have the same quality and morphology, the properties of the resulting crystalline heterojunction is decisively determined by the type of rod-like molecular layer underneath and connected interfacial electronic structure. Both *p*-6P and BP2T molecules act as perfect substrate layer inducing WEG of ZnPc. However, *p*-6P acts as a dielectric layer which blocks the holes coming from ZnPc, while BP2T enables good hole transport layer across the interface with ZnPc. This clearly demonstrates, that utilizing the weak-epitaxy growth method and selecting proper rod-like conjugated molecules as transparent or blocking layer, the hole transport characteristics in crystalline disklike/rodlike heterojunctions can be tuned, which is of vital importance for potential applications in crystalline organic devices and molecular solid-state circuits.

AUTHOR INFORMATION

Corresponding Author

*E-mail: m.knupfer@ifw-dresden.de. Tel: +49 351 4659544. Fax: +49 351 4659313.

ACKNOWLEDGMENT

We thank R. Hübel, S. Leger, and R. Schönfelder for technical assistance. Financial support by the Deutsche Forschungsgemeinschaft (Grants KN393/9 and KN393/14) is gratefully acknowledged.

REFERENCES

(1) Koller, G.; Berkebile, S.; Krenn, J. R.; Netzer, F. P.; Oehzelt, M.; Haber, T.; Resel, R.; Ramsey, M. G. *Nano Lett.* **2006**, *6*, 1207.
(2) Lunt, R. R.; Benziger, J. B.; Forrest, S. R. *Adv. Mater.* **2007**, *19*, 4229.
(3) Zhu, F.; Lou, K.; Huang, L.; Yang, J.; Zhang, J.; Wang, H.; Geng, Y.; Yan, D. *Appl. Phys. Lett.* **2009**, *95*, 203106.
(4) Simbrunner, C.; Quochi, F.; Hernandez-Sosa, G.; Oehzelt, M.; Resel, R.; Hesser, G.; Arndt, M.; Saba, M.; Mura, A.; Bongiovanni, G.; Sitter, H. *ACS Nano* **2010**, *4*, 6244.
(5) Zhang, Y.; Dong, H.; Tang, Q.; Ferdous, S.; Liu, F.; Mannsfeld, F. C. B.; Hu, W.; Briseno, A. L. *J. Am. Chem. Soc.* **2010**, *132*, 11580.
(6) Ishii, H.; Sugiyama, K.; Ito, E.; Seki, K. *Adv. Mater.* **1999**, *11*, 605.
(7) Salaneck, K. S. W. R.; Kahn, A.; Pireaux, J.-J. *Conjugated Polymer and Molecular Interfaces*; Marcel Dekker: New York, 2002.
(8) Cahen, D.; Kahn, A. *Adv. Mater.* **2003**, *15*, 271.
(9) Scott, J. C. *J. Vac. Sci. Technol., A* **2003**, *21*, 521.
(10) Knupfer, M.; Peisert, H. *Physica Status Solidi A* **2004**, *201*, 1055.
(11) Tang, J. X.; Lee, C. S.; Lee, S. T. *J. Appl. Phys.* **2007**, *101*, 064504.
(12) Koch, N. *J. Phys.: Condens. Matter* **2008**, *20*, 184008.
(13) Braun, S.; Salaneck, W. R.; Fahlman, M. *Adv. Mater.* **2009**, *21*, 1450.

(14) Hwang, J.; Wan, A.; Kahn, A. *Mater. Sci. Eng., R* **2009**, *64*, 1.
(15) Gao, Y. *Mater. Sci. Eng., R* **2010**, *68*, 39.
(16) Duhm, S.; Heimel, G.; Salzmann, I.; Glowatzki, H.; Johnson, R. L.; Vollmer, A.; Rabe, J. P.; Koch, N. *Nat. Mater.* **2008**, *7*, 326.
(17) Chen, W.; Huang, H.; Chen, S.; Huang, Y. L.; Gao, X. Y.; Wee, A. T. S. *Chem. Mater.* **2008**, *20*, 7017.
(18) Kakuta, H.; Hirahara, T.; Matsuda, I.; Nagao, T.; Hasegawa, S.; Ueno, N.; Sakamoto, K. *Phys. Rev. Lett.* **2007**, *98*, 247601.
(19) Koch, N.; Vollmer, A.; Salzmann, I.; Nickel, B.; Weiss, H.; Rabe, J. P. *Phys. Rev. Lett.* **2006**, *96*, 156803.
(20) Ding, H.; Reese, C.; Makinen, A. J.; Bao, Z.; Gao, Y. *Appl. Phys. Lett.* **2010**, *96*, 222106.
(21) Koller, G.; Berkebile, S.; Oehzelt, M.; Puschnig, P.; Ambrosch-Draxl, C.; Netzer, F. P.; Ramsey, M. G. *Science* **2007**, *317*, 351.
(22) Bao, Z.; Lovinger, A. J.; Dodabalapur, A. *Adv. Mater.* **1997**, *9*, 42.
(23) Leising, G.; Tasch, S.; Brandstatter, C.; Meghdadi, F.; Froyer, G.; Athouel, L. *Adv. Mater.* **1997**, *9*, 33.
(24) Yanagi, H.; Araki, Y.; Ohara, T.; Hotta, S.; Ichikawa, M.; Taniguchi, Y. *Adv. Funct. Mater.* **2003**, *13*, 767.
(25) Shirota, Y.; Kageyama, H. *Chem. Rev.* **2007**, *107*, 953.
(26) Wang, H.; Zhu, F.; Yang, J.; Geng, Y.; Yan, D. *Adv. Mater.* **2007**, *19*, 2168.
(27) Huang, L.; Liu, C.; Yu, B.; Zhang, J.; Geng, Y.; Yan, D. *J. Phys. Chem. B* **2010**, *114*, 4821.
(28) Hotta, S.; Kimura, H.; Lee, S. A.; Tamaki, T. *J. Heterocycl. Chem.* **2000**, *37*, 281.
(29) Garnier, F.; Horowitz, G.; Peng, X. Z. *Synth. Met.* **1991**, *45*, 163.
(30) Seah, M. P.; Dench, W. A. *Surf. Interface Anal.* **1979**, *1*, 2.
(31) Peisert, H.; Schwieger, T.; Knupfer, M.; Golden, A. S.; Fink, J. *J. Appl. Phys.* **2000**, *88*, 1535.
(32) Knupfer, M.; Paasch, G. *J. Vac. Sci. Technol., A* **2005**, *23*, 1072.
(33) Gao, W.; Kahn, A. *Org. Electron.* **2002**, *3*, 53.
(34) Gao, Y.; Ding, H.; Wang, H.; Yan, D. *Appl. Phys. Lett.* **2007**, *91*, 142112.
(35) Vázquez, H.; Gao, W.; Flores, F.; Kahn, A. *Phys. Rev. B* **2005**, *71*, 041306.
(36) Vázquez, H.; Flores, F.; Kahn, A. *Org. Electron.* **2007**, *8*, 241.
(37) Zhu, F.; Yang, J.; Song, D.; Li, C.; Yan, D. *Appl. Phys. Lett.* **2009**, *94*, 143305.
(38) Crone, B. K.; Davids, P. S.; Campbell, I. H.; Smith, D. L. *J. Appl. Phys.* **2000**, *87*, 1974.
(39) Horowitz, G. *J. Mater. Res.* **2004**, *19*, 1946.
(40) Yu, B.; Huang, L.; Wang, H.; Yan, D. *Adv. Mater.* **2010**, *22*, 1017.